Optimization and Characterization of TAPC:C60-Based Photomultiplication-Type Organic Photodetectors for Ultraviolet Detection

1st Sulaiman Hadi Hibatullah
School of Electrical Engineering
Telkom University
Bandung, Indonesia
sulaimanhadi@student.telkomuniversity.ac.id

2nd Husneni Mukhtar
School of Electrical Engineering
Universitas Telkom
Bandung, Indonesia
husnenimukhtar@telkomuniversity.ac.id

3rd Suksmandhira Harimurti
School of Electrical Engineering
Universitas Telkom
Bandung, Indonesia
suksmandhiraharimurti@telkomuniversity.ac.id

4th M. Rivaldi Ali Septian
School of Electrical Engineering
Universitas Telkom
Bandung, Indonesia
rivaldialiseptian@telkomuniversity.ac.id

Abstract—Photomultiplication-type organic photodetectors (PM-OPDs) are attractive for ultraviolet (UV) sensing because trapped charges can induce internal carrier injection and generate photocurrent gain. This manuscript condenses a thesis-based study of TAPC:C60 small-molecule PM-OPDs into an IEEE-style paper with corrected formulas, consistent units, and a detector-oriented interpretation. The devices were fabricated by vacuum thermal evaporation using the general architecture ITO/TAPC/TAPC:C60/TAPC/Ag. The active-layer blend ratio was fixed at TAPC:C60 = 50:1, while the variables were the anode-side TAPC hole-blocking layer (HBL) thickness and the TAPC:C60 active-layer thickness. Device performance was evaluated using dark current density, light current density, external quantum efficiency (EQE), spectral responsivity (SR), and specific detectivity (D*). The best overall configuration is Experiment 3A, ITO/TAPC 0 nm/TAPC:C60 100 nm/TAPC 5 nm/Ag 120 nm. At 330 nm and -12 V, this device achieved Jdark = 1.46154 × 10^{-8} A cm^{-2}, Jlight = 2.410 × 10^{-2} A cm^{-2}, EQE = 16109.87540%, SR = 42.87306 A W^{-1}, and D* = 6.26482 × 10^{14} Jones. Although the 70 nm active-layer device produced larger EQE and SR, the optimum detector was selected from the balance between photocurrent gain and suppressed dark-current noise.

***Keywords*—Organic photodetector, photomultiplication, EQE, responsivity, specific detectivity.**

I. INTRODUCTION

Ultraviolet radiation is an important optical stimulus in environmental monitoring, health protection, flame detection, sterilization control, and industrial safety. A UV detector must therefore convert UV photons into a measurable electrical signal while maintaining a low leakage baseline. This requirement is difficult because weak UV signals can be masked by dark current, thermally generated carriers, electrode injection, and trap-assisted leakage. For that reason, a UV detector should not be judged only by photocurrent or external quantum efficiency. It must also be assessed by noise-related parameters that determine whether weak optical signals can be resolved.

Organic photodetectors (OPDs) are relevant for this purpose because organic semiconductors can be deposited as thin films, engineered through molecular energy levels, and adapted for lightweight or large-area structures. Conventional photodiode-type OPDs usually operate without internal gain, so the collected carrier number is limited by photon absorption, exciton separation, and charge collection. Photomultiplication-type OPDs overcome this limitation by using trapped charges to promote additional carrier injection from the external circuit.

In PM-OPDs, photogenerated carriers are trapped at donor-acceptor sites or interfacial states. Under reverse bias, these trapped charges reshape the local electric field and thin the injection barrier. The increased probability of tunneling injection creates an amplified photocurrent, so the EQE can exceed 100%. However, the same field-assisted injection can also raise dark current if the structure is not controlled. Therefore, PM-OPD optimization requires a trade-off between gain and leakage.

The thesis dataset used in this paper focuses on TAPC:C60-based PM-OPDs for UV detection. TAPC functions as the donor-rich material and hole-transport pathway, while C60 acts as the electron acceptor and trapping component. The tested architecture is ITO/TAPC/TAPC:C60/TAPC/Ag, with variations in anode-side TAPC HBL thickness and active-layer thickness.

The main design question is not simply how to obtain the largest EQE. A 70 nm active layer can strengthen the electric field and produce large gain, but it can also increase reverse dark current. A thicker active layer or thicker HBL may reduce leakage, but it may also suppress useful photocurrent. This paper therefore selects the best model by specific detectivity D*, which combines responsivity and dark-current limitation.

The contribution of this manuscript is to present the thesis experiment in compact English form, correct the calculation flow and units, and explain why Experiment 3A, using no anode-side HBL and a 100 nm TAPC:C60

active layer, gives the most balanced UV detection performance at 330 nm and -12 V.

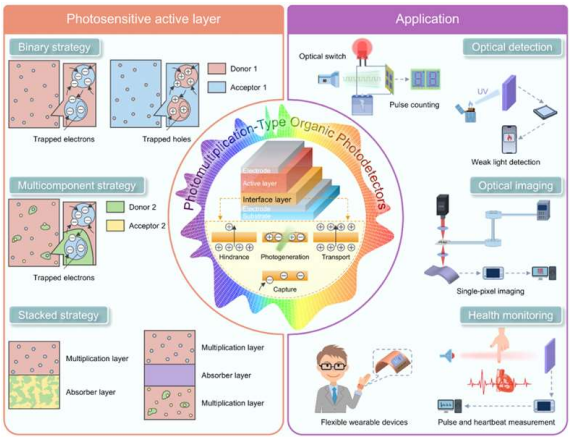


FIGURE 1
Photomultiplication-type organic photodetector concept and application context adapted from the thesis source figure.

II. DEVICE STRUCTURE AND PHOTOMULTIPLICATION MECHANISM

A. TAPC:C60 Device Architecture

The devices use a vertical sandwich architecture. The bottom electrode is 145 nm ITO, which acts as the transparent anode and optical entrance path. The anode-side TAPC layer is varied as an HBL with nominal thicknesses of 0 nm, 10 nm, or 20 nm. The active layer is a TAPC:C60 mixture with a 50:1 ratio and a thickness of either 70 nm or 100 nm. A 5 nm TAPC interlayer is then deposited near the Ag side, followed by a 120 nm Ag electrode.

Although TAPC is normally a hole-transport material, its role in this stack depends on position and carrier direction under reverse bias. When used as the anode-side layer, a thicker TAPC film can behave as a transport-limiting HBL. It can modify leakage and interfacial selectivity, but excessive thickness may reduce the useful light current. The HBL must therefore be optimized rather than simply increased.

The TAPC:C60 active layer is the region where UV absorption, exciton generation, charge separation, and trapping occur. C60 provides electron-accepting and trap-related sites, while the TAPC-rich matrix supports hole transport. Because the C60 fraction is low, the acceptor component promotes controlled trapping without forming a highly conductive electron pathway. This condition is central to photomultiplication behavior.

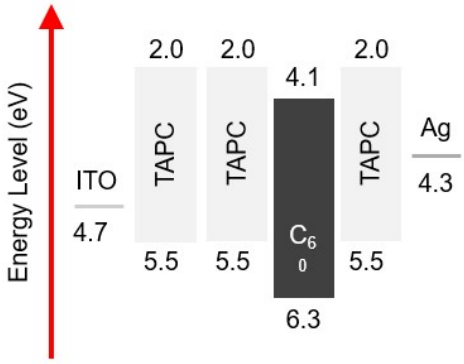


FIGURE 2
HOMO-LUMO energy-level diagram of the ITO/TAPC/TAPC:C60/TAPC/Ag structure used in the thesis.

B. Energy-Level Interpretation

The energy-level diagram uses approximate work functions of 4.7 eV for ITO and 4.3 eV for Ag. TAPC is represented by LUMO = 2.0 eV and HOMO = 5.5 eV, while C60 is represented by LUMO = 4.1 eV and HOMO = 6.3 eV. These levels favor electron transfer from photoexcited TAPC toward C60. Trapped electrons then create a local field that bends the energy levels and assists injection under reverse bias.

This picture explains both the benefit and the risk of PM-OPDs. Under illumination, trapped electrons can thin the injection barrier and increase tunneling-assisted carrier injection. In the dark, strong reverse bias or poorly controlled interfaces may activate leakage through similar barrier-lowering paths. The optimum device is therefore not the structure with maximum gain alone, but the structure that keeps gain useful while limiting dark-current noise.

For this reason, EQE and SR are treated as response indicators, while D* is used as the main detector-quality indicator. D* increases with responsivity but decreases when Jdark rises, making it more appropriate for weak-light UV sensing.

C. Photomultiplication Sequence

The photomultiplication process begins when a UV photon is absorbed in the TAPC:C60 active layer and forms an exciton. Donor-acceptor interaction assists exciton dissociation: electrons move toward C60-related states, while holes remain in the TAPC-rich phase. A portion of the electrons becomes trapped at C60 or interfacial states.

These trapped electrons reshape the interfacial barrier. Under reverse bias, the local field from trapped charge and the applied field jointly enhance band bending and tunneling probability. Additional carriers are then injected from the external circuit, producing photocurrent larger than the primary photogenerated current. This explains the very high EQE values observed in the UV region.

The gain process must remain controlled. Too much injection increases dark current, while an overly resistive HBL or active layer suppresses the useful signal. PM-OPD optimization is therefore a balance among trapping, field distribution, charge transport, and leakage suppression.

III. EXPERIMENTAL METHOD

A. Experimental Matrix

The experimental matrix consists of three groups. Experiment 1 uses a 70 nm TAPC:C60 active layer with a 10 nm TAPC HBL. Experiment 2 compares 10 nm and 20 nm HBL layers while keeping the active layer at 100 nm. Experiment 3 compares 0 nm and 10 nm HBL configurations with the same 100 nm active layer. All devices retain a 5 nm TAPC interlayer near Ag and a 120 nm Ag electrode.

The TAPC:C60 ratio is fixed at 50:1 so that the analysis emphasizes layer-thickness effects. The selected best model is Experiment 3A, ITO/TAPC 0 nm/TAPC:C60 100 nm/TAPC 5 nm/Ag 120 nm. This configuration removes the anode-side HBL while maintaining the 100 nm active layer and Ag-side TAPC interlayer.

TABLE 1
DEVICE CONFIGURATIONS EVALUATED IN THE THESIS DATASET

Config.	ITO	HBL TAPC	Active Layer	TAPC Interlayer	Ag
Exp. 1	145 nm	10 nm	TAPC:C60 50:1, 70 nm	5 nm	120 nm
Exp. 2A	145 nm	10 nm	TAPC:C60 50:1, 100 nm	5 nm	120 nm
Exp. 2B	145 nm	20 nm	TAPC:C60 50:1, 100 nm	5 nm	120 nm
Exp. 3A	145 nm	0 nm	TAPC:C60 50:1, 100 nm	5 nm	120 nm
Exp. 3B	145 nm	10 nm	TAPC:C60 50:1, 100 nm	5 nm	120 nm

B. Fabrication Route

The devices are fabricated by vacuum thermal evaporation. ITO substrates are cleaned and transferred into the fabrication environment. TAPC, C60, and Ag are placed in separate evaporation sources, and the chamber is pumped to high vacuum to reduce oxygen, moisture, and residual gas collisions that can disturb film quality or thickness uniformity.

The TAPC:C60 layer is formed by co-deposition. Deposition rates are controlled to obtain the 50:1 blend ratio after tooling correction. The thesis records tooling values of 44 for TAPC, 270 for C60 in the active-layer adjustment, and 60 for Ag. Tooling correction is needed because the quartz-crystal sensor and the substrate do not always receive identical material flux.

After the organic layers are deposited, Ag is evaporated through the cathode mask to form the top contact. The completed devices are handled carefully and encapsulated to reduce oxygen and moisture exposure before characterization.

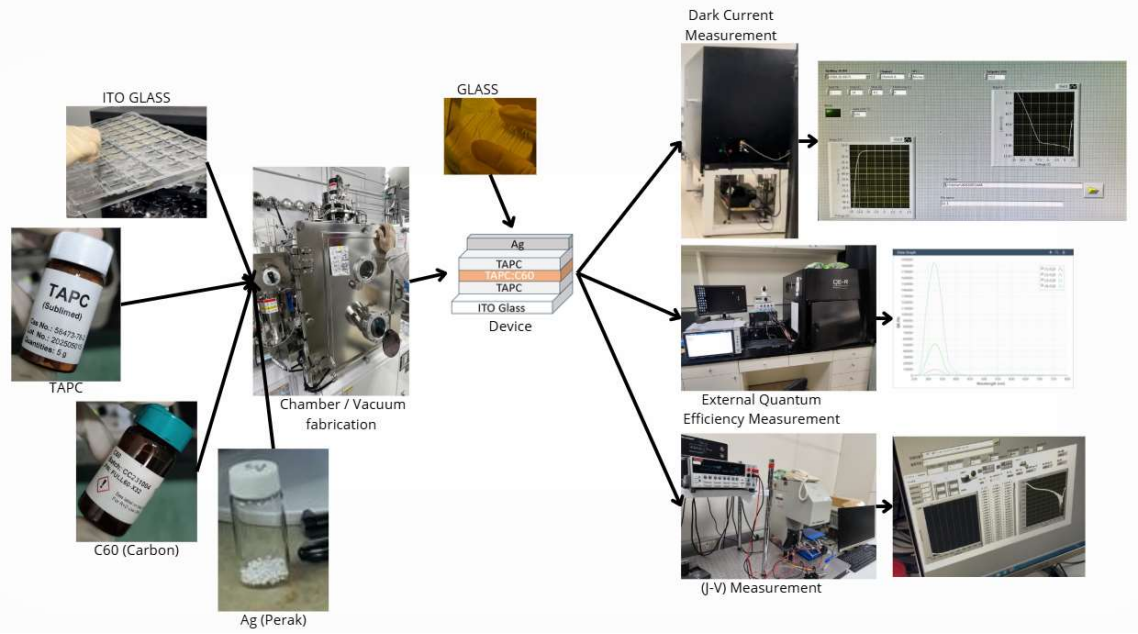


FIGURE 3
Fabrication and characterization route for the TAPC:C60 PM-OPD devices.

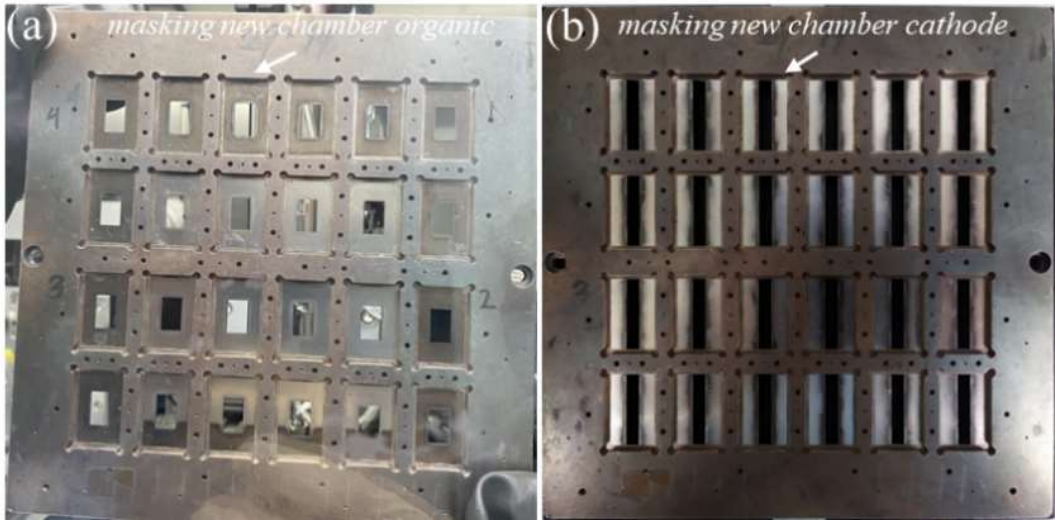


FIGURE 4
Organic and cathode masks used during the vacuum thermal evaporation process.

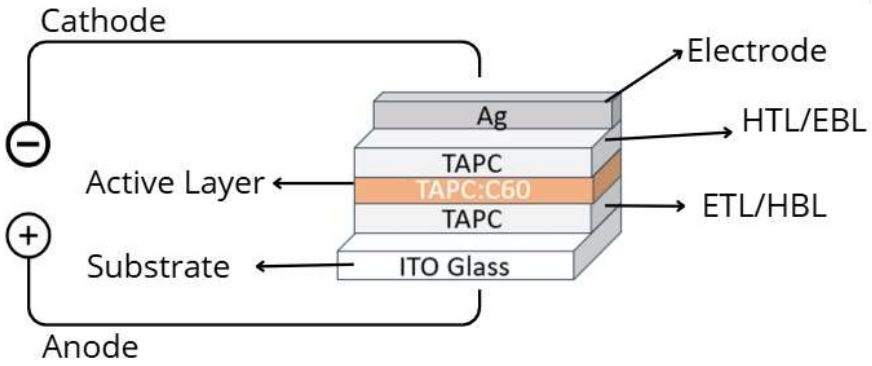


FIGURE 5
Layer stack of the ITO/TAPC/TAPC:C60/TAPC/Ag PM-OPD structure.

C. Characterization Procedure

Dark current is measured in a dark box using a source-measure unit. The device is biased from the positive region toward reverse bias, and the measured current is normalized by active area. This parameter represents baseline leakage and is used as the dark-current input for shot-noise-limited D* calculation.

Light current is measured under illumination. Because the illuminated current contains both leakage and optical response, the photocurrent density is obtained by subtracting Jdark from Jlight. EQE and responsivity are then calculated from this photocurrent density, not from the raw light current alone.

EQE and SR are evaluated as wavelength-dependent parameters, with the main comparison focused on 330 nm at -8 V, -10 V, -12 V, and -14 V. Numerical processing is used to calculate the performance parameters, while spectral graphs are used to compare bias and structure effects.

IV. PERFORMANCE PARAMETERS AND CORRECTED FORMULAS

The formulas follow one calculation flow: measured currents are normalized into current density, photocurrent is obtained by subtracting the dark component, and SR, EQE, and D* are calculated from Jph and Jdark. The active area is denoted by A in cm². Current density is reported in A cm^{-2}, responsivity in A W^{-1}, and detectivity in Jones.

Dark current density is the leakage current density measured without illumination:

$$J_{dark} = I_{dark} / A \quad (1)$$

where Idark is the measured dark current and A is the active area.

Light current density is the current density measured under illumination:

$$J_{light} = I_{light} / A \quad (2)$$

where Ilight is the measured illuminated current.

The useful photocurrent density is calculated as:

$$Jph = J_{light} - J_{dark} \quad (3)$$

where Jph is the net light-induced current density used for SR and EQE.

Spectral responsivity describes output photocurrent density per incident optical power density:

$$R(\lambda) = J_{ph}(\lambda) / P_{in}(\lambda) \quad (4)$$

where Pin is the incident optical power density in W cm^{-2}.

External quantum efficiency compares collected charge carriers with incident photons:

$$EQE(\lambda) = [J_{ph}(\lambda)\, h\, c] / [q\, P_{in}(\lambda)\, \lambda] \times 100\% \quad (5)$$

where h is Planck's constant, c is the speed of light, q is the elementary charge, and λ is wavelength. In PM-OPDs, EQE may exceed 100% because the collected carrier number is amplified by trap-assisted injection.

Specific detectivity is calculated using the shot-noise-limited approximation:

$$D^* = R / \sqrt{(2\, q\, J_{dark})} \quad (6)$$

This expression shows that D* improves with higher responsivity but decreases when Jdark increases.

TABLE 2
SYMBOLS, DEFINITIONS, AND UNITS USED IN THE CORRECTED FORMULAS

Symbol	Definition	Formula Role	Unit
A	Active device area	Current normalization	cm^2
Jdark	Dark current density	I_dark/A	A cm^{-2}
Jlight	Light current density	Ilight/A	A cm^{-2}
Jph	Photocurrent density	Jlight - Jdark	A cm^{-2}
P_in	Incident optical power density	Input to SR and EQE	W cm^{-2}
R or SR	Spectral responsivity	Jph/P_in	A W^{-1}
EQE	External quantum efficiency	(Jphhc)/(qP_inλ) × 100%	%
D*	Specific detectivity	$R/(2qJdark)^{1/2}$	Jones

V. RESULTS

A. Pixel Selection and Dark-Current Screening

Each fabricated sample contains several active pixels. Different pixels may show different dark-current behavior because of local variations in deposition uniformity, contact quality, or microscopic defects. The thesis therefore selects the tested pixel by considering both the numerical Jdark value and the stability of the J-V curve.

This screening is important because all later parameters are calculated from the selected active point. An unstable pixel may distort EQE, SR, and D*. For Experiment 3A, the selected HBL-free configuration gives Jdark = 1.46154 × 10^{-8} A cm^{-2} and Jlight = 2.410 × 10^{-2} A cm^{-2} at -12 V, which supports high detectivity.

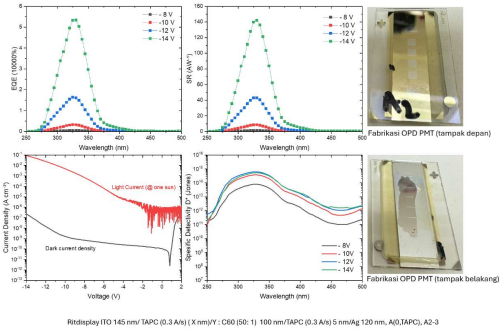


FIGURE 6
Complete best-model characterization panel for Experiment 3A, including EQE, SR, current density, D*, and device images.

B. Experiment 1: 70 nm Active Layer with 10 nm HBL

Experiment 1 uses ITO/TAPC 10 nm/TAPC:C60 70 nm/TAPC 5 nm/Ag 120 nm. At 330 nm and -12 V, it gives Jlight = 0.06527 A cm^{-2}, Jdark = 2.18221 × 10^{-6} A cm^{-2}, EQE = 51052.88800%, SR = 135.86656 A W^{-1}, and D* = 1.62478 × 10^{14} Jones. At -14 V, the EQE increases to 180560.81100%, and SR reaches 480.52474 A W^{-1}.

The strong EQE and SR are attributed to the shorter 70 nm active layer, which increases the effective electric field and assists carrier collection and tunneling injection. However, the same structure also produces much higher dark current than the 100 nm devices. Its D* is therefore below the best HBL-free 100 nm device despite its larger gain.

Thus, the 70 nm device is best described as the strongest gain configuration, not the best detector configuration. Its result proves that high photomultiplication must be evaluated together with leakage.

C. Experiment 2: HBL 10 nm versus 20 nm at 100 nm Active Layer

Experiment 2 keeps the active layer at 100 nm and changes the anode-side TAPC HBL from 10 nm to 20 nm. At 330 nm and -12 V, Device A with 10 nm HBL reaches EQE = 8352.24255%, SR = 22.22774 A W^{-1}, and D* = 5.37807 × 10^{14} Jones. Device B with 20 nm HBL reaches EQE = 3135.21870%, SR = 8.34373 A W^{-1}, and D* = 1.95894 × 10^{14} Jones.

Increasing the HBL thickness from 10 nm to 20 nm reduces the photoresponse. Although a thicker HBL can suppress some leakage paths, it also increases the barrier for useful transport. Because the signal current decreases strongly, D* also decreases.

This confirms that the HBL thickness must be optimized. In this dataset, 20 nm TAPC is too restrictive, while 10 nm gives a better compromise between selectivity and photocurrent.

D. Experiment 3: HBL 0 nm versus 10 nm at 100 nm Active Layer

Experiment 3 compares the HBL-free structure and the 10 nm HBL structure at 100 nm active-layer thickness. Experiment 3A uses ITO/TAPC 0 nm/TAPC:C60 100 nm/TAPC 5 nm/Ag 120 nm, while Experiment 3B uses the same structure with a 10 nm TAPC HBL.

At 330 nm and -12 V, Experiment 3A produces EQE = 16109.87540%, SR = 42.87306 A W^{-1}, and D* = 6.26482 × 10^{14} Jones. Experiment 3B produces EQE = 12010.83528%, SR = 31.96432 A W^{-1}, and D* = 4.41852 × 10^{14} Jones. The HBL-free structure therefore gives the stronger response and the higher detectivity.

The superiority of Experiment 3A is associated with field distribution and interface transport. Removing the anode-side HBL reduces one organic interface and allows the reverse-bias field to act more directly across the TAPC:C60 active layer. The 100 nm thickness still prevents dark current from reaching the high level observed in the 70 nm device.

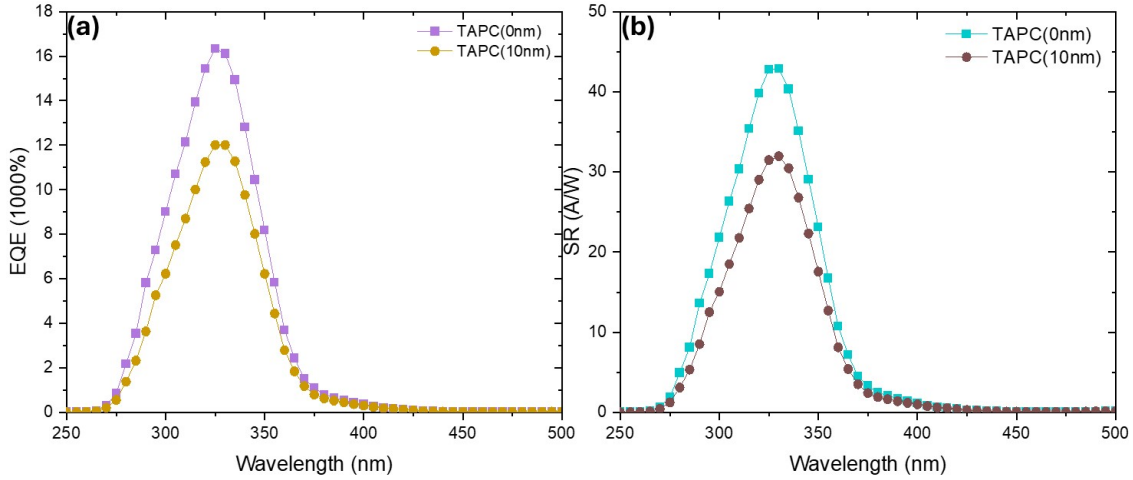


FIGURE 7
Spectral EQE and SR comparison for Experiment 3 devices with 0 nm and 10 nm HBL.

TABLE3
PERFORMANCE COMPARISON AT 330 nm AND -12 V

Config.	Jlight (A cm^{-2})	Jdark (A cm^{-2})	EQE (%)	SR (A W^{-1})	D* (Jones)
Exp. 1	6.527×10^{-2}	2.18221×10^{-6}	51052.88800	135.86656	1.62478×10^{14}
Exp. 2A	1.021×10^{-2}	5.33087×10^{-9}	8352.24255	22.22774	5.37807×10^{14}
Exp. 2B	7.310×10^{-3}	5.66157×10^{-9}	3135.21870	8.34373	1.95894×10^{14}
Exp. 3A	2.410×10^{-2}	1.46154×10^{-8}	16109.87540	42.87306	6.26482×10^{14}
Exp. 3B	2.381×10^{-2}	1.63319×10^{-8}	12010.83528	31.96432	4.41852×10^{14}

E. Bias Dependence of the Best Model

For Experiment 3A, EQE and SR increase as reverse bias rises from -8 V to -14 V. This is expected because a stronger reverse field supports exciton separation, carrier extraction, and trap-assisted tunneling injection. Nevertheless, the best D* occurs at -12 V rather than -14 V.

At -8 V, D* is 7.92896×10^{13} Jones. At -10 V, it increases to 3.69125×10^{14} Jones. At -12 V, it reaches 6.26482×10^{14} Jones. At -14 V, EQE and SR continue to increase, but Jdark rises to 2.25528×10^{-7} A cm^{-2}, so D* decreases to 5.28782×10^{14} Jones.

This result confirms that the optimum operating voltage is not necessarily the largest reverse bias. For the best model at 330 nm, -12 V gives the most favorable balance between gain and dark-current noise.

TABLE4
BIAS-DEPENDENT PERFORMANCE OF EXPERIMENT 3A AT 330 nm

Config.	Jlight (A cm^{-2})	Jdark (A cm^{-2})	EQE (%)	SR (A W^{-1})	D* (Jones)
-8 V	6.99679×10^{-4}	1.81747×10^{-10}	444.17567	1.18208	7.92896×10^{13}
-10 V	4.83×10^{-3}	1.63562×10^{-9}	3175.35367	8.45054	3.69125×10^{14}
-12 V	2.410×10^{-2}	1.46154×10^{-8}	16109.87540	42.87306	6.26482×10^{14}
-14 V	6.129×10^{-2}	2.25528×10^{-7}	53414.01302	142.15020	5.28782×10^{14}

VI. CROSS-CONFIGURATION ANALYSIS

A. Active-Layer Thickness Effect

The comparison between 70 nm and 100 nm active layers shows the effect of transport distance and electric-field distribution. The 70 nm layer gives stronger field-assisted gain and the highest EQE and SR, especially in the UV response around 330 nm.

However, the 70 nm device also shows higher dark current. A shorter transport path helps photocarrier extraction, but it also makes reverse injection easier in the dark. The 100 nm layer reduces leakage and becomes more favorable when combined with the proper HBL condition.

Therefore, active-layer optimization must consider both gain and leakage. The 70 nm device is suitable as a high-gain reference, while the HBL-free 100 nm device is more suitable for weak-light UV detection.

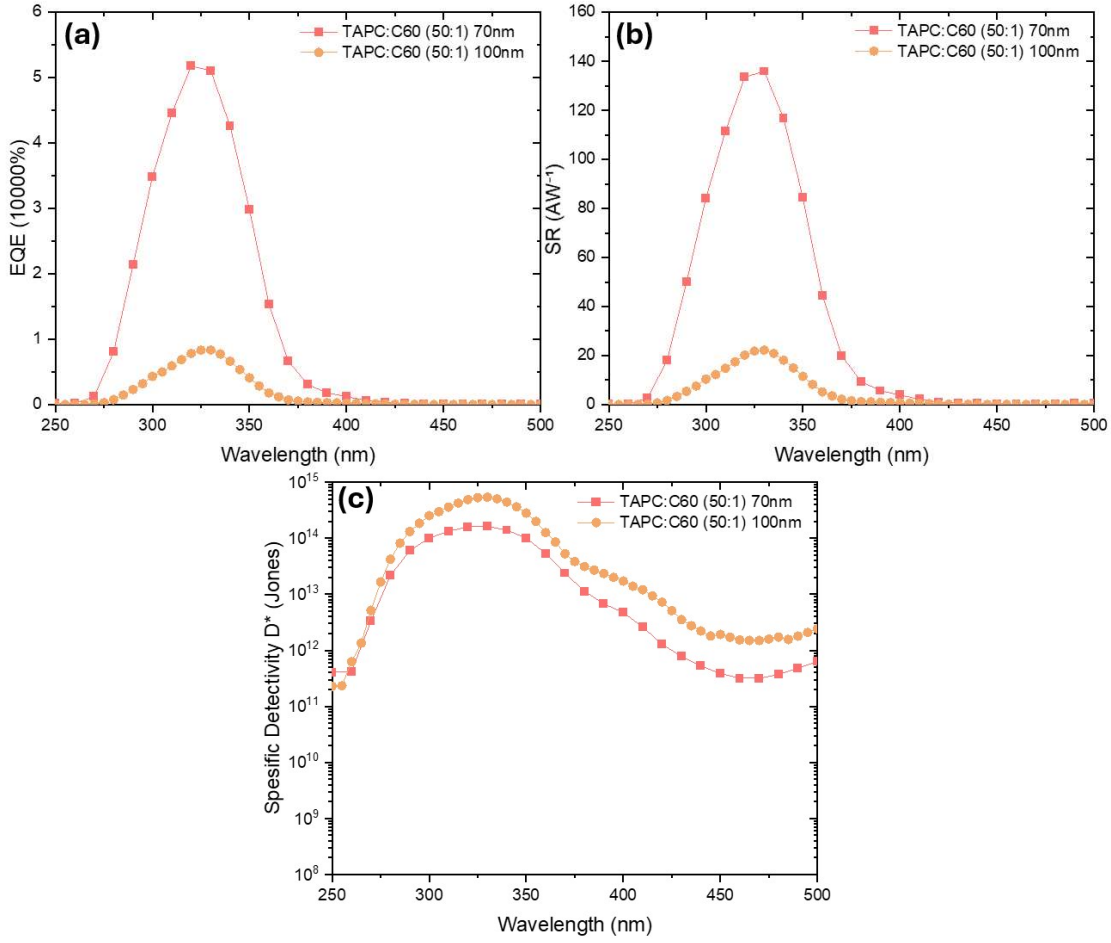


FIGURE 8
Comparison of EQE, SR, and D* for 70 nm and 100 nm active-layer configurations.

B. HBL Thickness Effect

The HBL comparison shows that the HBL-free configuration gives the best total performance among the 100 nm devices. The 0 nm HBL device achieves the highest EQE, SR, and D* at the selected operating point. The 10 nm HBL still performs well, while the 20 nm HBL suppresses the response too strongly.

This does not mean that HBL layers are always detrimental. It means that in this particular stack, composition, and fabrication condition, the anode-side TAPC layer is not the optimum interface. If the electrode work function, surface treatment, or active-layer composition changes, the optimum HBL thickness may also change.

The physical interpretation is consistent with the energy-level diagram. Without the anode-side HBL, the active layer couples more directly to ITO and to the reverse-bias

field. C60-related trapping still promotes band bending, while the 100 nm layer limits excessive leakage. This balance explains the high D* at -12 V.

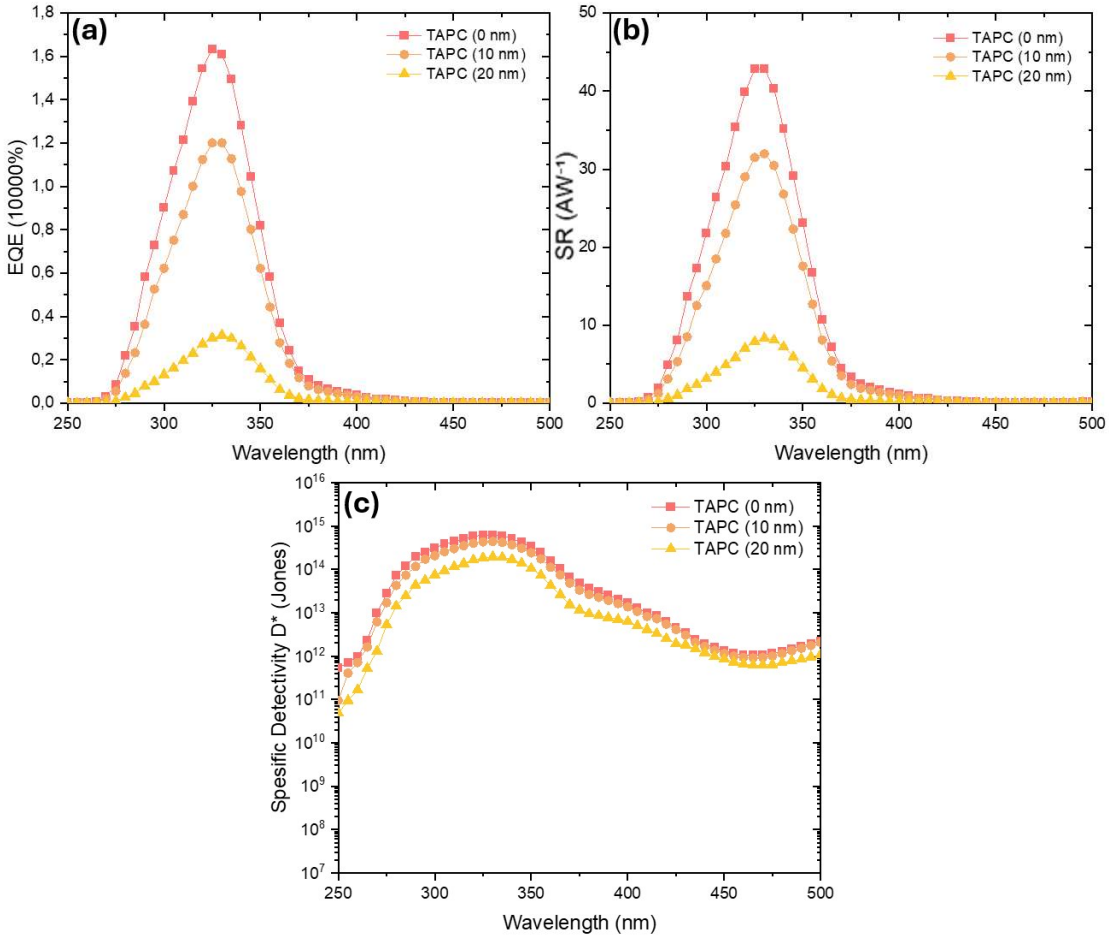


FIGURE 9
HBL-thickness comparison showing the dominant performance of the 0 nm HBL structure.

C. Current-Density Balance

Light current density describes the signal under illumination, while dark current density describes leakage and noise. A device with high Jlight but very high Jdark may show large EQE yet still be unsuitable for weak-light detection. A device with very low Jdark but weak Jlight can also give limited sensitivity.

Experiment 3A provides the best balance in the dataset. It does not have the highest Jlight, but it maintains strong photocurrent while keeping Jdark controlled. This is why its D* is the highest.

For practical UV sensing, operating conditions should be selected using D* and the intended light-intensity range. In this study, -12 V operation of Experiment 3A is the most appropriate point for high UV detectivity at 330 nm.

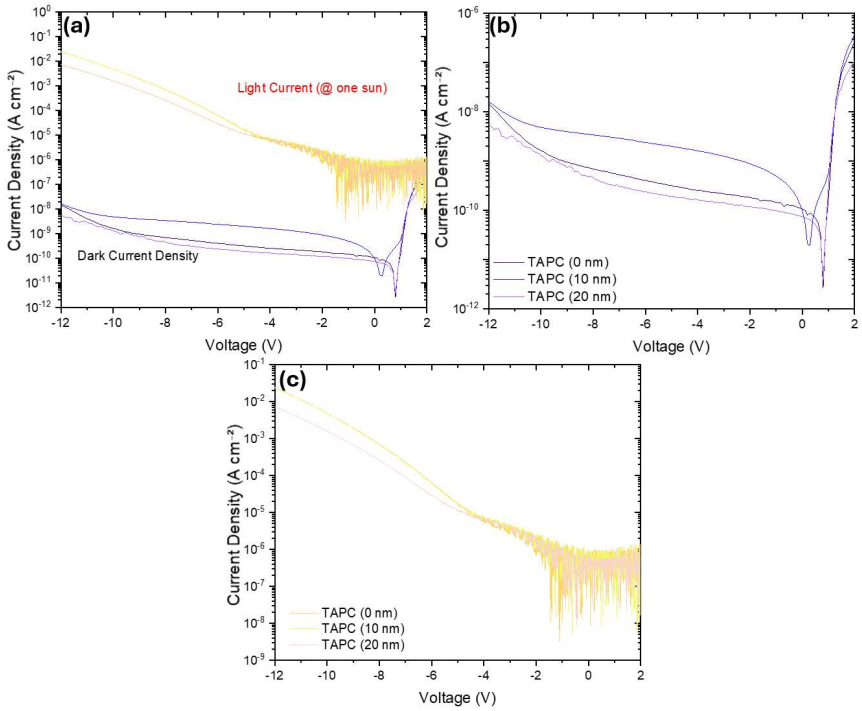


FIGURE 10
Current-density comparison across HBL configurations, emphasizing the trade-off between signal and leakage.

VII. DISCUSSION

The results show that photomultiplication is useful only when internal gain does not create excessive leakage. In a PM-OPD, trapped charge intentionally modifies the interfacial barrier so that additional carriers are injected. This can raise EQE far beyond 100%, but it can also increase dark current if the field distribution and interface condition are not balanced.

Experiment 1 illustrates the high-gain side of the trade-off. Its 70 nm active layer gives the largest EQE and SR, but its dark current is much higher than in the 100 nm devices. Therefore, it is not the best detector when the objective is weak-light sensitivity. Experiment 2 shows the opposite risk: a thicker 20 nm HBL restricts useful charge transport so strongly that D* decreases even though leakage is not the worst case.

Experiment 3A achieves the most favorable compromise. Removing the anode-side TAPC HBL improves carrier transport and allows the reverse-bias field to modulate the TAPC:C60 layer more effectively. At the same time, the 100 nm active layer prevents leakage from becoming excessive. C60-related trapping still supports band bending and tunneling injection under illumination, producing high SR and the highest D* at -12 V.

The decrease in D* at -14 V is important because it proves that the highest bias is not automatically the best operating point. EQE and SR continue to rise, but the increase in Jdark strengthens the shot-noise term and lowers detectivity. A detector-oriented optimization must therefore prioritize the signal-to-noise balance rather than gain alone. This balance is especially relevant for UV sensing, where small optical signals must remain distinguishable from bias-induced leakage during practical reverse-bias operation conditions.

The present analysis is limited to dark current density, light current density, EQE, responsivity, and shot-noise-limited D*. Direct noise spectral density, response time, linear dynamic range, long-term stability, humidity response, aging behavior, and repeated-device statistics were not included. Future work should add direct noise measurement, morphology analysis, repeated fabrication, and interface engineering so that the link between film quality, trapping, leakage, and detectivity can be verified more completely.

From an engineering perspective, the most useful next step is to reduce reverse-bias leakage while preserving trap-assisted gain. Possible strategies include controlled acceptor distribution, improved interface treatment, optimized active-layer thickness, better encapsulation, and statistical pixel-to-pixel evaluation.

VIII. CONCLUSION

This paper condenses the TAPC:C60 PM-OPD thesis dataset into an English IEEE-style manuscript with corrected formulas, consistent units, source figures, and a detector-oriented interpretation. The evaluated devices use the general structure ITO/TAPC/TAPC:C60/TAPC/Ag with variations in HBL thickness and active-layer thickness.

The corrected calculation flow is based on $J_{dark} = I_{dark}/A$, $J_{light} = I_{light}/A$, $J_{ph} = J_{light} - J_{dark}$, $R = J_{ph}/P_{in}$, $EQE = (J_{ph}hc)/(qP_{in}\lambda) \times 100\%$, and $D^* = R/\sqrt{(2qJ_{dark})}$. Current density is reported in A cm^{-2}, responsivity in A W^{-1}, EQE in %, and D* in Jones.

The 70 nm active-layer device gives the strongest gain, with EQE = 51052.88800% and SR = 135.86656 A W^{-1} at 330 nm and -12 V. However, its higher dark current limits its D*. The best overall model is Experiment 3A, ITO/TAPC 0 nm/TAPC:C60 100 nm/TAPC 5 nm/Ag 120 nm. At 330 nm and -12 V, it achieves Jdark = 1.46154 × 10^{-8} A cm^{-2}, Jlight = 2.410 × 10^{-2} A cm^{-2}, EQE = 16109.87540%, SR = 42.87306 A W^{-1}, and D* = 6.26482 × 10^{14} Jones.

The final conclusion is that the optimum TAPC:C60 PM-OPD is determined by the balance between photomultiplication gain and dark-current suppression. EQE and SR remain important response metrics, but D* is the strongest selection parameter for weak-light UV detection. Based on this criterion, the HBL-free 100 nm active-layer configuration is the most promising device in the thesis dataset.

ACKNOWLEDGMENT

The author acknowledges Telkom University, the thesis supervisors, and the laboratory team involved in the PM-OPD fabrication and characterization process.

REFERENCES

[1] J. Wang, Z. Liu, T. Zhu, Z. Kang, X. Zeng, B. Zhou, Y. Zhou, J. Mu, and Z. Yin, "Strategies for achieving high-performance photomultiplication-type organic photodetectors and their promising applications," Nano Energy, vol. 132, 110399, 2024, doi: 10.1016/j.nanoen.2024.110399.

[2] M. Hiramoto, T. Imahigashi, and M. Yokoyama, "Photocurrent multiplication in organic pigment films," Applied Physics Letters, vol. 64, pp. 187-189, 1994, doi: 10.1063/1.111527.

[3] J. Miao and F. Zhang, "Recent progress on photomultiplication type organic photodetectors," Laser & Photonics Reviews, vol. 13, 1800204, 2019, doi: 10.1002/lpor.201800204.

[4] Z. Zhao, C. Xu, L. Niu, X. Zhang, and F. Zhang, "Recent progress on broadband organic photodetectors and their applications," Laser & Photonics Reviews, vol. 14, 2000262, 2020, doi: 10.1002/lpor.202000262.

[5] H. Ren, J.-D. Chen, Y.-Q. Li, and J.-X. Tang, "Recent progress in organic photodetectors and their applications," Advanced Science, vol. 8, 2002418, 2021, doi: 10.1002/advs.202002418.

[6] R. D. Jansen-van Vuuren, A. Armin, A. K. Pandey, P. L. Burn, and P. Meredith, "Organic photodiodes: the future of full color detection and image sensing," Advanced Materials, vol. 28, pp. 4766-4802, 2016, doi: 10.1002/adma.201505405.

[7] Y. Fang, A. Armin, P. Meredith, and J. Huang, "Accurate characterization of next-generation thin-film photodetectors," Nature Photonics, vol. 13, pp. 1-4, 2019, doi: 10.1038/s41566-018-0288-z.

[8] A. H. Fallahpour, S. Kienitz, and P. Lugli, "Origin of dark current and detailed description of organic photodiode operation under different illumination intensities," IEEE Transactions on Electron Devices, vol. 64, no. 6, pp. 2649-2654, 2017, doi: 10.1109/TED.2017.2691000.

[9] J. Kublitski, A. Hofacker, T. Boroujeni, B. Lüssem, and K. Leo, "Reverse dark current in organic photodetectors and the major role of traps as source of noise," Nature Communications, vol. 12, 551, 2021, doi: 10.1038/s41467-020-20856-z.

[10] G. Simone, D. Di Carlo Rasi, X. de Vries, G. H. L. Heintges, S. C. J. Meskers, R. A. J. Janssen, and G. H. Gelinck, "Organic photodetectors and their application in large area and flexible image sensors: the role of dark current," Advanced Functional Materials, vol. 30, 1904205, 2020, doi: 10.1002/adfm.201904205.

[11] D. Guo, L. Yang, J. Zhao, J. Li, G. He, D. Yang, L. Wang, A. Vadim, and D. Ma, "Visible-blind ultraviolet narrowband photomultiplication-type organic photodetector with an ultrahigh external quantum efficiency of over 1000000%," Materials Horizons, vol. 8, pp. 2293-2302, 2021, doi: 10.1039/D1MH00776A.

[12] L. Li, F. Zhang, J. Wang, Q. An, Q. Sun, W. Wang, J. Zhang, and F. Teng, "Achieving EQE of 16700% in P3HT:PC71BM based photodetectors by trap-assisted photomultiplication," Scientific Reports, vol. 5, 9181, 2015, doi: 10.1038/srep09181.

[13] L. Li, F. Zhang, W. Wang, Q. An, J. Wang, Q. Sun, and M. Zhang, "Trap-assisted photomultiplication polymer photodetectors obtaining an external quantum efficiency of 37500%," ACS Applied Materials & Interfaces, vol. 7, pp. 5890-5897, 2015, doi: 10.1021/acsami.5b00041.

[14] L. Li, F. Zhang, W. Wang, Y. Fang, and J. Huang, "Revealing the working mechanism of polymer photodetectors with ultra-high external quantum efficiency," Physical Chemistry Chemical Physics, vol. 17, pp. 30712-30720, 2015, doi: 10.1039/C5CP05557A.

[15] W. Wang, F. Zhang, M. Du, L. Li, M. Zhang, K. Wang, Y. Wang, B. Hu, Y. Fang, and J. Huang, "Highly narrowband photomultiplication type organic photodetectors," Nano Letters, vol. 17, pp. 1995-2002, 2017, doi: 10.1021/acs.nanolett.6b05418.

[16] J. Wang and Q. Zheng, "Enhancing the performance of photomultiplication-type organic photodetectors using solution-processed ZnO as an interfacial layer," Journal of Materials Chemistry C, vol. 7, pp. 1544-1550, 2019, doi: 10.1039/C8TC04962A.

[17] S. H. Hibatullah, "Analisis karakterisasi perangkat fotodetektor organik berbasis fotomultiplikasi dalam mendeteksi cahaya ultraviolet," Undergraduate Thesis, School of Electrical Engineering, Telkom University, Bandung, Indonesia, 2026.